GNSS based Attitude determination with Statistical and Deterministic Baseline A Priori Information

P. Jurkowski[*,**], P. Henkel[*,**] and C. Günther[**,***]
[*] *Advanced Navigation Solutions - ANAVS, Gilching, Germany*
[**] *Technische Universität München (TUM), Munich, Germany*
[***] *German Aerospace Center (DLR), Oberpfaffenhofen, Germany*

BIOGRAPHIES

Patryk Jurkowski studied electrical engineering and information technology at the Technische Universität München, Munich, Germany. He completed his bachelor of science in 2010 and received his diploma with a thesis on „Reliable attitude determination with GNSS: Gaussian a priori knowledge and Kalman filtering“ with distinction in 2011. He also received the first prize in Bavaria in the European Satellite Navigation competition in 2010 for a differential carrier phase positioning system. Patryk worked as a student trainee on EGNOS performance and integrity for Galileo at EADS Astrium from 2006 to 2010. He founded Advanced Navigation Solutions - ANAVS in 2011.

Patrick Henkel received his Bachelor, Master and PhD degrees from the Technische Universität München, Munich, Germany. In 2010, he graduated with a PhD thesis on reliable carrier phase positioning, which received with ”summa cum laude“ the highest distinction. Patrick is now working towards his habilitation in the field of precise point positioning. He visited the Mathematical Geodesy and Positioning group at TU Delft in 2007, and the GPS Lab at Stanford University in 2008 and 2010. Patrick received the Pierre Contensou Gold Medal at the International Astronautical Congress in 2007, the first prize in Bavaria at the European Satellite Navigation Competition in 2010, and the Vodafone Award for his dissertation in 2011. He is one of the founders and currently also the managing director of Advanced Navigation Solutions - ANAVS.

Christoph Günther studied theoretical physics at the Swiss Federal Institute of Technology in Zurich. He received his diploma in 1979 and completed his PhD in 1984. He worked on communication and information theory at Brown Boveri and Ascom Tech. From 1995, he led the development of mobile phones for GSM and later dual mode GSM/Satellite phones at Ascom. In 1999, he became head of the research department of Ericsson in Nuremberg. Since 2003, he is the director of the Institute of Communication and Navigation at the German Aerospace Center (DLR) and since December 2004, he additionally holds a Chair at the Technische Universität München (TUM). His research interests are in satellite navigation, communication and signal processing.

ABSTRACT

Attitude determination with carrier phase measurements is becoming increasingly popular for maritime and automobile navigation. However, multipath, frequent loss of lock, cycle slips and severe clock drifts prevent reliable integer ambiguity resolution especially for low-cost GNSS receivers. The reliability of carrier phase ambiguity resolution can be improved by a few methods: One option is the use of some baseline a priori information to reduce the integer search space. This a priori information can be given either in a deterministic or stochastic (Jurkowski [1], Jurkowski et al. [2], Henkel et al. [3]) form. Another option is the use of multi-frequency linear combinations, which increase the wavelength to noise ratio and, thereby, reduce the number of grid points within the search space volume. A third option is the use of state space models, which exploit the inertia of the vehicles and can be efficiently implemented by recursive least-squares estimation/ Kalman filtering. Finally, one can include additional measurements from inertial sensors and/ or further antennas, and perform an on-board calibration of double difference measurements.

In this paper, a method is proposed that uses precise carrier phases for attitude determination without the need of ambiguity resolution: First, a synchronization of double difference measurements is performed by computing a range correction based on the satellite movement within the receiver differential clock offset time. Secondly, if the receiver is moving on a straight path, a linear least-squares fitting of a sequence of absolute code-based position solutions gives an estimate of the path direction and, thus, an on-board calibration of double difference measurements can be even performed with the help of the baseline length, pitch and roll angle a priori information and

satellite-receiver direction vectors. The calibrated carrier phases can then be coasted without the need of ambiguity resolution. The observed accuracy is $0.5°/$ baseline length, i.e. $0.5°$ for a baseline length of 1 m an $0.005°$ for a baseline length of 100 m.

The proposed algorithm was tested with real measurements from two low-cost, single frequency u-blox LEA 6T receivers mounted on the roof of a car and compared with the high precision INS/GPS coupled navigation system iTraceRT-F400 of iMAR as a reference sensor. The measurement results show that our kinematic calibration of the double difference phases provides a heading accuracy that is sufficient for most applications.

Secondly, a Maximum Likelihood (ML) and Maximum A posteriori Probability (MAP) estimation of ambiguities and baselines is proposed. These estimators find the optimum trade-off between an estimator that minimizes only the range residuals (e.g. unconstrained LAMBDA) and one, which minimizes only the distance to the a priori information. The Gaussian a priori knowledge of the baseline length, pitch, roll and yaw angles serves as a soft constraint, i.e. it gives a certain preference direction but allows some uncertainties in the a priori knowledge. Consequently, the MAP estimation of ambiguities and baselines is faster than the unconstrained LAMBDA and also more robust than the constrained LAMBDA, which uses a deterministic a priori information. The Gaussian a priori information is fully integrated into the float solution, into the integer search (by inequality constraints), and into the fixed baseline solution.

INTRODUCTION

Attitude determination based on GNSS is an interesting alternative/ supplement to inertial navigation systems (INS). Inertial navigation sensors enable an accurate positioning during short GPS outages but suffer from drifts, biases and colored noise, which are difficult to model properly. As GNSS provides a drift-free position estimate, it is commonly used to calibrate INS.

This paper focuses on attitude determination solely based on GNSS measurements from single frequency low cost receivers and antennas: Two LEA-6T receivers were used, which include temperature compensated crystal oscillators (TCXO) and correspond to the newest GPS-receiver series (with raw data output) of u-blox. The antennas were low-cost patch antennas with 10 MHz bandwidth and an integrated low noise amplifier with 27 dB gain. These receivers suffer from frequent phase jumps due to unreliable tracking, severe code multipath, substantial antenna phase center variations, and clock oscillations that are too large to be canceled by double differencing.

For automobile applications, the baseline length is just around 1 m, which makes the use of carrier phase measurements indispensable for attitude determination. However, carrier phase measurements are ambiguous, and the development of methods for their reliable resolution has received a lot of attraction during the last years. Approaches include the coupling of GNSS and INS measurements, the use of multi-frequency linear combinations to increase the ambiguity discrimination [4, 5, 6], the introduction of a priori knowledge [7, 2], and the use of multi-antenna systems. Ambiguity resolution uses the code and carrier phase measurements as provided by the delay locked loop and phase locked loop. Note that the integer search is not discussed in this paper as it is described in detail in [8, 9, 10].

CALIBRATION OF DOUBLE DIFFERENCE CARRIER PHASE MEASUREMENTS

Low cost GNSS receivers with single frequency L1 patch antennas can often not track the carrier phase reliably in kinematic urban environments. Multipath results in frequent loss of locks and cycle slips as shown in Fig. 1 for some exemplary measurements. To assure a reliable attitude determination based on double differenced carrier phases, a fast and precise on-board phase calibration is necessary. A

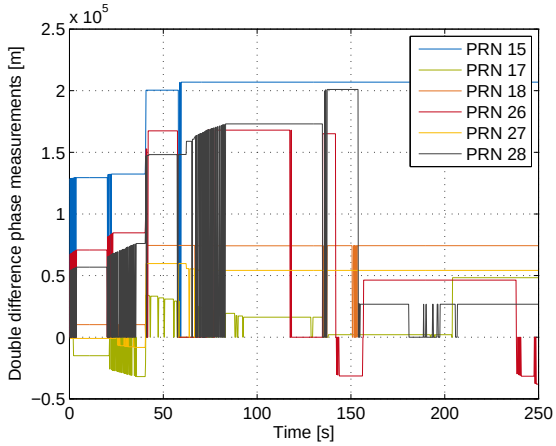

Fig. 1 Low-cost receivers, such as the u-blox LEA 6T, are not able to track the carrier phase continuously. These loss' of lock are responsible for the severity of ambiguity resolution with classical methods.

robust on-board calibration technique was developed and tested for a scenario where just the heading is estimated since knowledge about the heading is sufficient for most land based applications. Our method benefits from using the precise carrier phase without the requirement of ambiguity resolution. The calibration can be performed whenever the receiver is moving on a straight line which is approximately two orders of magnitude larger than the baseline length, such that the heading can be derived from a set of absolute position solutions. This straight line is almost always given at the scenario discussed here, i.e. a car moving in urban and rural environments as shown in Fig. 2 and Fig. 3. The straight line was automatically detected by the algorithm and is marked with a solid red line between point (1)

and (2) in both figures. The heading information together

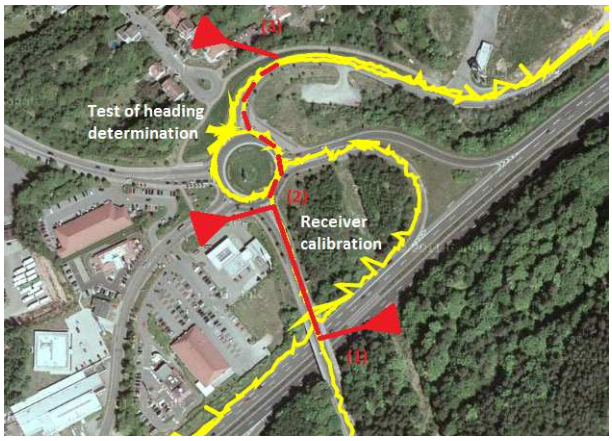

Fig. 2 On-board calibration of two GNSS receivers - test I: The yellow track shows the absolute position solutions, that are heavily affected by code multipath. The double difference carrier phases are calibrated between (1) and (2), where the baseline and straight street are aligned. Afterwards, the heading is exclusively derived from the calibrated carrier phases.

with an a priori knowledge about the baseline length and pitch angle enable a calibration of the double differenced carrier phases. Thus, this calibration technique consists of two components, i.e. the determination of phase corrections and the coasting.

In detail, the method starts with a computation of absolute code-based position solutions from a few epochs and then transforms these absolute ECEF coordinates into geodetic coordinates, i.e. longitude λ, latitude φ and height h. Afterwards, a linear least-squares fitting of the latitudes as a function of longitudes is performed. The parameters p_0 and p_1 of the fitted polynomial

$$p(\lambda) = p_0 + p_1\lambda \tag{1}$$

are determined such that

$$\min_{p_0,p_1} \sum_i \left(p(\lambda(t_i)) - \varphi(t_i)\right)^2 \tag{2}$$

holds true for the set of given $(\lambda(t_i), \varphi(t_i))$ tuples. This minimization can also be written in matrix-vector notation as

$$\min_{\begin{bmatrix}p_0\\p_1\end{bmatrix}} \| \underbrace{\begin{bmatrix}1 & \lambda(t_1)\\ 1 & \lambda(t_2)\\ \vdots & \vdots\\ 1 & \lambda(t_n)\end{bmatrix}}_{\boldsymbol{V}} \underbrace{\begin{bmatrix}p_0\\p_1\end{bmatrix}}_{\boldsymbol{p}} - \underbrace{\begin{bmatrix}\varphi(t_1)\\ \varphi(t_2)\\ \vdots\\ \varphi(t_n)\end{bmatrix}}_{\boldsymbol{\varphi}} \|^2, \tag{3}$$

where $\boldsymbol{V}$ is a Vandermonde matrix. The least-squares estimates of the polynomial coefficients $\boldsymbol{p}$ follow as

$$\boldsymbol{p} = \left(\boldsymbol{V}^T\boldsymbol{V}\right)^{-1}\boldsymbol{V}^T\boldsymbol{p}. \tag{4}$$

Figure 4 shows the linear interpolation of the trajectory of a receiver moving on a straight line where the dots represent the code-based measurements of the latitude/ longitude tuples and p_0 and p_1 are the parameters of the linear interpolation. The polynomial fitting can be in general applied to the position coordinates in any coordinate system. However, a geodetic coordinate system is favorable, because it enables a separation of the more precise horizontal components from the less precise height.

In a second step, we fix the position of one receiver to a point $\{\lambda_{f,1},\ \varphi_{f,1} = p_0 + p_1\lambda_{f,1}\}$ on the polynomial as shown in Fig. 4, and search for the coordinates $\{\lambda_{f,2} = \lambda_{f,1} + \Delta\lambda,\ \varphi_{f,2} = p_0 + p_1\lambda_{f,2}\}$ of the second receiver on the polynomial under the constraint of a given baseline length $\bar{l}$. This is equivalent to solving the equation

$$\begin{aligned} f(\Delta\lambda) &= \|\hat{\vec{x}}_1 - \hat{\vec{x}}_2\left(\lambda_{f,2}, \varphi_{f,2}, h_2\right)\|^2 - \bar{l}^2 \\ &= \|\hat{\vec{x}}_1 - \hat{\vec{x}}_2\left(\lambda_{f,1} + \Delta\lambda,\right. \\ &\quad \left. p_0 + p_1(\lambda_{f,1} + \Delta\lambda), h_2\right)\|^2 \\ &\quad -\bar{l}^2 \stackrel{!}{=} 0, \end{aligned} \tag{5}$$

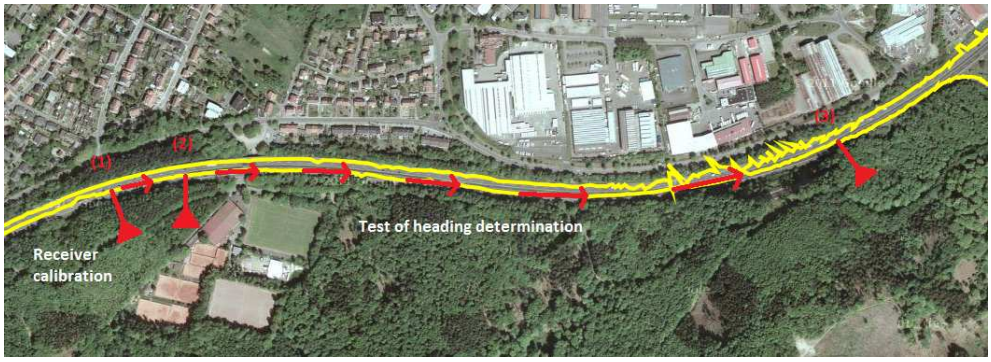

Fig. 3 On-board calibration of two GNSS receivers - test II: The calibration was performed within $4\mathrm{s}$ on highway A6 near St. Ingbert (Germany) at a speed of approximately $100\mathrm{km/h}$. The calibrated carrier phases were then coasted over $40\mathrm{s}$ corresponding to a distance of approx. $1\mathrm{km}$. The computed heading estimates are shown in Fig. 7.

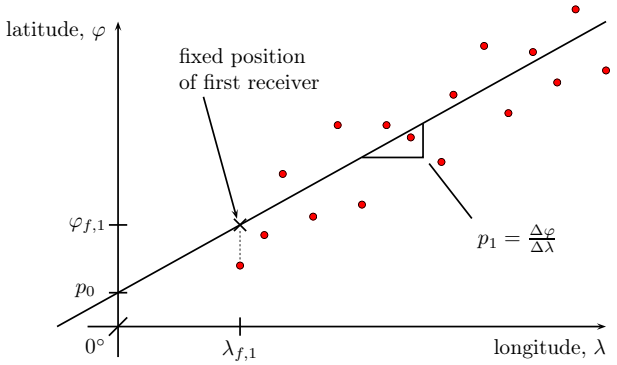

Fig. 4 The code-based measurements of a receiver moving on a straight with its linear interpolation

for $\Delta\lambda$, using the well-known transformation of geodetic coordinates into ECEF coordinates [11, 12]:

$$\hat{\vec{x}}_r(\lambda_r, \varphi_r, h_r) = \begin{bmatrix} \hat{x}_{\mathrm{ECEF},r} \\ \hat{y}_{\mathrm{ECEF},r} \\ \hat{z}_{\mathrm{ECEF},r} \end{bmatrix} = \begin{bmatrix} (N_{\varphi_r} + h_r)\cos(\varphi_r)\cos(\lambda_r) \\ (N_{\varphi_r} + h_r)\cos(\varphi_r)\sin(\lambda_r) \\ \left(N_{\varphi_r}\left(1-e^2\right) + h_r\right)\sin(\varphi_r) \end{bmatrix}, \tag{6}$$

with e being the eccentricity of the earth. The root finding problem of (5) is also indicated in Fig. 5, i.e. the position of the second receiver is chosen such that it fulfills the baseline length requirement in the Cartesian (ECEF) coordinate system and also lies on the polynomial defined in the geodetic coordinate system.

Replacing $\hat{\vec{x}}_r(\lambda_r, \varphi_r, h_r), r \in \{1, 2\}$, in (5) by (6) yields

$$\begin{aligned} f(\Delta\lambda) = &\left(\hat{x}_{\mathrm{ECEF},1} - \left(N_{\varphi_{f,2}} + h_2\right)\right. \\ &\cdot \cos\left(p_0 + p_1\left(\lambda_{f,1} + \Delta\lambda\right)\right)\cos\left(\lambda_{f,1} + \Delta\lambda\right)\Big)^2 \\ &+ \left(\hat{y}_{\mathrm{ECEF},1} - \left(N_{\varphi_{f,2}} + h_2\right)\right. \\ &\cdot \cos\left(p_0 + p_1\left(\lambda_{f,1} + \Delta\lambda\right)\right)\sin\left(\lambda_{f,1} + \Delta\lambda\right)\Big)^2 \\ &+ \left(\hat{z}_{\mathrm{ECEF},1} - \left(N_{\varphi_{f,2}}\left(1-e^2\right) + h_2\right)\right. \\ &\cdot \sin\left(p_0 + p_1\left(\lambda_{f,1} + \Delta\lambda\right)\right)\Big)^2 - \bar{l}^2 = 0, \end{aligned} \tag{7}$$

where $\Delta\lambda$ is the only unknown variable. As Eq. (7) can not be solved in closed form for $\Delta\lambda$, the roots of $f(\Delta\lambda)$ are computed iteratively with the Gauss-Newton method:

$$\Delta\lambda_{n+1} = \Delta\lambda_n - \left.\frac{f(\Delta\lambda)}{f'(\Delta\lambda)}\right|_{\Delta\lambda=\Delta\lambda_n}, \tag{8}$$

where the derivative $f'(\Delta\lambda)$ can be derived from (7) in closed form. Once $\Delta\lambda$ is known, the baseline vector can be calibrated with (6) to

$$\begin{aligned} \hat{b} = &\hat{x}_1(\lambda_{f,1}, \varphi_{f,1}, h_1) \\ &- \hat{x}_2(\lambda_{f,1} + \Delta\lambda, p_0 + p_1(\lambda_{f,1} + \Delta\lambda), h_2), \end{aligned} \tag{9}$$

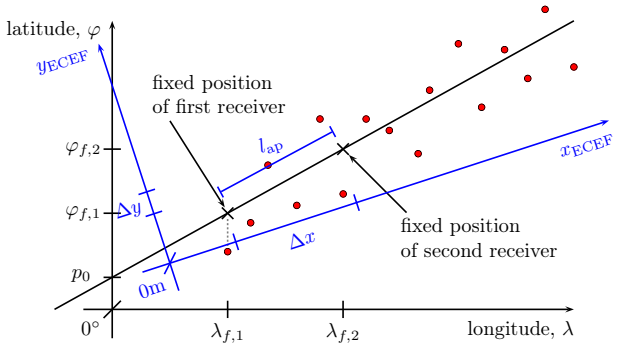

Fig. 5 The position of the second receiver is fixed by searching a point that lies on the trajectory given in Ellipsoidal coordinates and in addition fulfills the constraint of a priori known baseline length given in ECEF coordinates

which lies on the polynomial and simultaneously fulfills the a priori length constraint.

Finally, the double difference (DD) carrier phase measurement at time t_i is calibrated to

$$\Delta\varphi^{kl}_{\mathrm{cal}}(t_i) = (\Delta\vec{e}^{\,kl}(t_i))^T\hat{b}(t_i). \tag{10}$$

The calibration correction is determined by averaging the difference of the measured and calibrated double difference phases over N_{cal} epochs, i.e.

$$\delta\varphi^{kl}_{\mathrm{corr}} = \frac{1}{N_{\mathrm{cal}}} \cdot \sum_{i=1}^{N_{\mathrm{cal}}} \left(\Delta\varphi^{kl}(t_i) - \Delta\varphi^{kl}_{\mathrm{cal},12}(t_i)\right), \tag{11}$$

which requires a continuous tracking for N_{cal} epochs. The calibration correction is then subtracted from the measurements of all upcoming measurements, i.e. the measurements are calibrated to

$$\Delta\varphi^{kl}_{\mathrm{cal}}(t_i) = \Delta\varphi^{kl}(t_i) - \delta\varphi^{kl}_{\mathrm{corr}} \quad \forall\, i > N_{\mathrm{cal}}. \tag{12}$$

Fig. 6 and Fig. 7 show a comparison of the heading estimates based on calibrated double difference carrier phases and a sequence of absolute position solutions. The calibration was performed within 10 s in the urban environment. Afterwards, the carrier phases were coasted, i.e. no further calibration or adjustment was performed. Obviously, the coasted carrier phases result in a much less noisy and less multipath affected heading information. The length of the baseline was 1.078 m, the pitch angle was 0°.

A measurement campaign was performed, where the heading estimate of presented algorithm for carrier phase calibration and coasting was compared to the heading estimate of the high precision INS/GPS coupled navigaion system iTraceRT-F400 of iMAR as a reference sensor. A Novatel high-end GPS receiver was used to prevent a drift of the inertial sensor. An accuracy of $\sigma_x = 2\mathrm{cm}$ for the absolute position and $\sigma_\nu = 0.01°$ for roll, pitch and heading was achieved with this INS/GPS combination. The inertial reference sensor was mounted to the body of the rear trunk

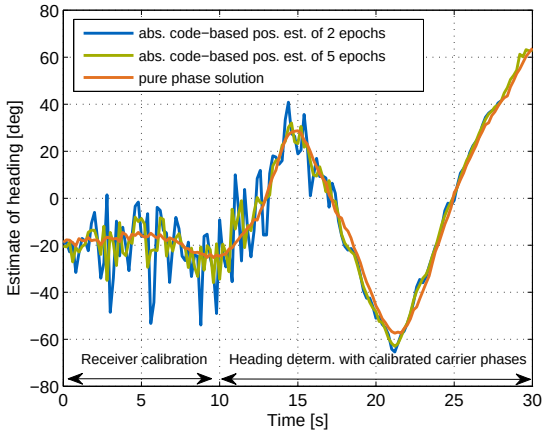

Fig. 6 Estimation of heading at roundabout: The heading can be determined with a significantly higher precision from calibrated double difference carrier phase measurements than from a sequence of absolute code-based position solutions. One can also observe that the coasted carrier phases do not drift within the considered time-span.

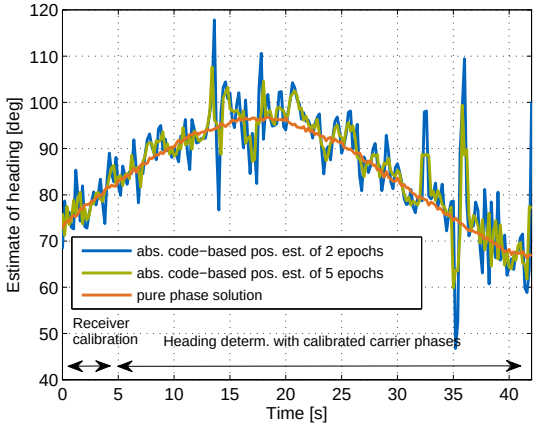

Fig. 7 Estimation of heading on highway: The higher speed enables a faster carrier phase calibration. The coasting of carrier phases results again in a significantly less noisy heading information compared to one derived from a sequence of absolute code-based position solutions

of a car as shown in the left picture of Fig. 8. The Novatel reference antenna together with the low-cost L1 patch antennas were installed on the roof of the same car as shown in the right picture of Fig. 8. Each of the L1 patch antennas was connected to a LEA-6T GPS module of u-blox.

Fig. 9 shows the comparison of heading estimation from presented algorithm and the heading estimation of the INS/GPS reference sensor from iMAR. The observable difference of $1^\circ - 2^\circ$ between both systems can be explained with the variation of the antenna phase center and an imperfect placement of both u-blox antennas on the roof of the car which leads to a baseline that is not aligned in direction of the longitudinal axis of the car. The carrier phases were calibrated during the first five seconds, where it is not possible to recognize a difference in performance with respect to the adjacent coasting of calibrated phases. This can be explained with the large scale of shown heading and the fact that the carrier phases were calibrated and coasted prior to the period shown in Fig. 9.

A more accurate comparison of heading estimation is shown in Fig. 10, where the difference of heading estimation between the carrier phase based attitude estimation and the INS/GPS reference attitude estimation is plotted for the same period of time as in the previous Fig. 9. In addition, the constant bias observed in previous figure was eliminated manually, on the ground that an error caused by an imperfect placement of both antennas is not of interest in our consideration. Note that the slightly higher difference during the first five seconds can be explained by the calibration which takes place at this period. Additionally, a standard deviation lower than a half degree can be observed for the difference in estimated heading at the period of adjacent coasting of calibrated phases and a baseline length

Fig. 8 Measurement equipment: The left picture shows the iTraceRT-F400 and iTraceRT-F200 of iMAR mounted in the rear trunk. The right picture shows the roof with the white Novatel antenna and the two smaller u-blox antennas in the front and at the rear. The baseline length between both u-blox receivers was $1.078\mathrm{m}$

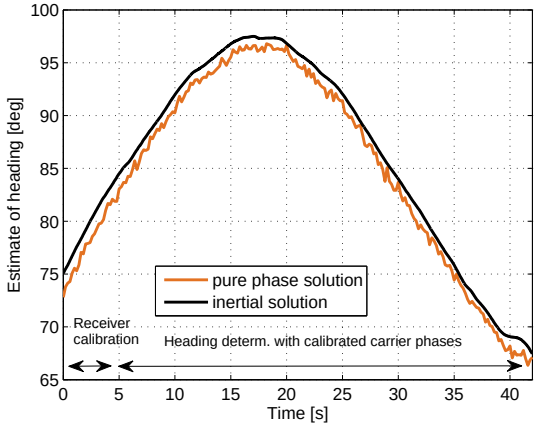

Fig. 9 Comparison of heading estimation of carrier phase based solution and heading estimation of the INS/GPS reference sensor. The first five seconds show the calibration period and the remaining period shows the coasting of calibrated carrier phases.

of 1.078m

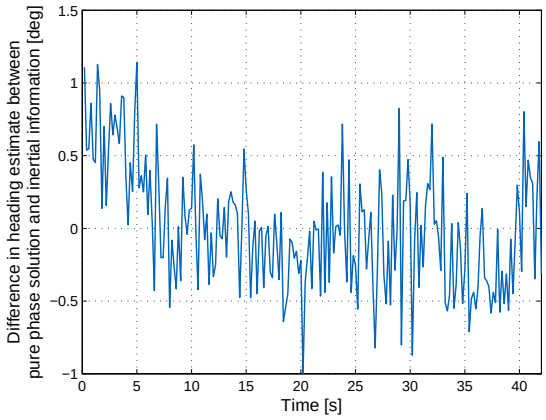

Fig. 10 Difference between heading estimation of carrier phase based technique and the INS/GPS reference sensor. The noise of about 1° can be explained with the short baseline compared to the noise of the carrier phase.

Cycle slip detection and correction

Multipath and shadowing might reduce the signal power, which leads to phase jumps of an integer multiple of $\lambda/2$. These cycle slips shall be detected on a single satellite basis by computing the difference between the measured double difference phase at epoch t_i and the extrapolated double difference phase at epoch t_i, i.e.

$$\begin{aligned}\delta\varphi^{kl}(t_i) &= \Delta\varphi^{kl}(t_i) - \Delta\varphi^{kl}_{\mathrm{pred}}(t_i) \\ &= \Delta\varphi^{kl}(t_i) - \big(\Delta\varphi^{kl}(t_{i-2} + 2(t_{i-1} - t_{i-2}) \\ &\quad \cdot \frac{\Delta\varphi^{kl}(t_{i-1}) - \Delta\varphi^{kl}(t_{i-2})}{t_{i-1} - t_{i-2}}\Big), \end{aligned} \quad (13)$$

where the extrapolation is based here on the measurements of the last two epochs but could also take a larger history into account. Dividing the phase offset of (13) by $\lambda/2$ and rounding to the nearest integer number yields

$$\check{N}^{kl}(t_i) = \left[\frac{\delta\varphi^{kl}(t_i)}{\lambda/2}\right]. \quad (14)$$

A cycle slip is detected if this number differs from zero and if two further constraints are fulfilled: First, the remaining real-valued offset has to be below a certain threshold (e.g. 1.5 cm) to support the integer nature of cycle slips, i.e.

$$|\delta\varphi^{kl}(t_i) - \frac{\lambda}{2}\check{N}^{kl}| < \Delta\varphi_{\mathrm{th}}, \quad (15)$$

and, secondly, the receiver velocity has to be above a certain minimum value v_{th} as for low velocities the receiver might suddenly change its direction of movement and, thereby, causes naturally much larger gradients in the double difference phase.

Once a cycle slip is detected, it can be easily removed from the measurements by

$$\Delta\varphi^{kl}_{\mathrm{corr}}(t_i) = \Delta\varphi^{kl}(t_i) - \frac{\lambda}{2}\check{N}^{kl}(t_i). \quad (16)$$

Detection of other phase jumps and correction based on extrapolated phases

If the criterion (15) is not fulfilled, then the phase jump can not be considered as a cycle slip. However, it might still be corrected based on the history of the phase as long as a continuous tracking was available over at least $N_{\mathrm{ep,min}}$ epochs. In this case, a polynomial of order l is fitted into the last $N_{\mathrm{ep,min}}$ phases, i.e.

$$\min_{p_0,\ldots,p_l} \sum_{j=1}^{N_{\mathrm{ep,min}}} \big(\Delta\varphi^{kl}(t_{i-j}) - (p_0 + p_1 t_{i-j} + \ldots + p_l t^l_{i-j})\big)^2 \quad (17)$$

and then used to extrapolate the phase to the "jumping" epoch, i.e.

$$\Delta\varphi^{kl}_{\mathrm{cal}}(t_i) = p_0 + p_1 t_i + \ldots + p_l t_i. \quad (18)$$

Note that this single satellite based correction of phase jumps can be again only performed if the receiver is moving sufficiently fast as for low velocities the receiver might suddenly change its direction of movement and, thereby, naturally cause a large gradient in the double difference phase.

One-dimensional iterative heading determination

The calibrated double difference phase measurements can be written in matrix-vector notation as

$$\Delta\boldsymbol{\varphi}_{\mathrm{cal}} = \underbrace{\begin{bmatrix} (\vec{e}^{\,12})^T \\ \vdots \\ (\vec{e}^{\,1K})^T \end{bmatrix}}_{\boldsymbol{H}} \boldsymbol{R}_{\substack{\mathrm{ENU} \\ \mathrm{ECEF}}} \begin{bmatrix} l\cos(\nu_1)\cos(\nu_2) \\ l\cos(\nu_1)\sin(\nu_2) \\ l\sin(\nu_1) \end{bmatrix} + \boldsymbol{\eta}, \tag{19}$$

where $\boldsymbol{H}$ includes the single difference unit vectors pointing from the satellites to the receiver in ECEF coordinates, $\boldsymbol{R}_{\substack{\mathrm{ENU} \\ \mathrm{ECEF}}}$ describes the transformation of local into ECEF coordinates, l is the baseline length, ν_1 is the pitch angle/ elevation and ν_2 denotes the heading.

Assuming that the baseline length is a priori known (i.e. $l = \bar{l}$) and that the pitch angle is $\nu_1 = 0°$ (which is in general valid for maritime and automotive applications), (19) can be further developed to

$$\Delta\boldsymbol{\varphi}_{\mathrm{cal}} = \tilde{\boldsymbol{H}} \begin{bmatrix} \bar{l}\cos(\nu_2) \\ \bar{l}\sin(\nu_2) \\ 0 \end{bmatrix} + \boldsymbol{\eta}, \tag{20}$$

with $\tilde{\boldsymbol{H}}$ being implicitly defined by (19) and (20). As the estimation of ν_2 is a non-linear problem, the trigonometric functions are linearized around an initial value $\nu_{2,0}$, i.e.

$$\begin{aligned} \cos(\nu_2) &\approx \cos(\nu_{2,0}) - \sin(\nu_{2,0}) \cdot (\nu_2 - \nu_{2,0}) \\ \sin(\nu_2) &\approx \sin(\nu_{2,0}) + \cos(\nu_{2,0}) \cdot (\nu_2 - \nu_{2,0}) \end{aligned} \tag{21}$$

to transform (20) into a measurement that depends linearly on the heading ν_2:

$$\begin{aligned} \Delta\tilde{\boldsymbol{\varphi}}_{\mathrm{cal}} &= \Delta\boldsymbol{\varphi}_{\mathrm{cal}} - \tilde{\boldsymbol{H}} \begin{bmatrix} \bar{l}\cos(\nu_{2,0}) + \bar{l}\sin(\nu_{2,0}) \cdot \nu_{2,0} \\ \bar{l}\sin(\nu_{2,0}) - \bar{l}\cos(\nu_{2,0}) \cdot \nu_{2,0} \\ 0 \end{bmatrix} \\ &= \tilde{\boldsymbol{H}} \cdot \bar{l} \begin{bmatrix} -\sin(\nu_{2,0}) \\ \cos(\nu_{2,0}) \\ 0 \end{bmatrix} \cdot \nu_2 + \boldsymbol{\eta} = \tilde{\boldsymbol{h}} \cdot \nu_2 + \boldsymbol{\eta}. \end{aligned} \tag{22}$$

The least-squares estimation of ν_2 then easily follows as

$$\hat{\nu}_2 = \left(\tilde{\boldsymbol{h}}^T \tilde{\boldsymbol{h}}\right)^{-1} \tilde{\boldsymbol{h}}^T \Delta\tilde{\boldsymbol{\varphi}}_{\mathrm{cal}}. \tag{23}$$

This estimate is then used to make a new linearization of ν_2 around $\hat{\nu}_2$, and then to re-compute $\Delta\tilde{\boldsymbol{\varphi}}_{\mathrm{cal}}$ and $\hat{\nu}_2$. Further iterations might be made although simulations have shown that a sufficient convergence is achieved within two iterations. The initial value $\nu_{2,0}$ at epoch t_i is typically chosen as the converged value $\hat{\nu}_2(t_{i-1})$ of the previous epoch.

This heading estimation was tested with two low cost u-blox LET 6T receivers, which were mounted on the roof of a car. Both receivers were aligned with the direction of movement, and the distance between both cars was $1.078\mathrm{m}$. Fig. 3 shows the route of the vehicle, which starts with a straight highway section used for calibrating the phases of all satellites, and a subsequent slightly curved highway section, during which the heading is derived solely from the coasted carrier phases.

Fig. 7 shows the obtained heading estimates for the predescribed algorithm in comparison to the heading estimates that one would obtain from the code/ pseudorange-based position estimates. The heading was referred to the North direction and counted clockwise, i.e. the initial value of the heading is $70°$, which corresponds to a movement essentially in Eastern direction with a small North component. One can easily observe in Fig. 7 that the proposed algorithm enables a much more precise heading estimate than the code-based solution as our approach is solely based on the carrier phase, which is tracked with a centimeter accuracy and much less affected by multipath.

Instantaneous re-calibration of newly tracked satellites

The carrier phase of a rising satellite can be instantaneously calibrated with the help of the already calibrated carrier phases. This instantaneous calibration of one double difference is based on (24), which shall be reused in this case:

$$\Delta\varphi^{kl}_{\mathrm{cal}}(t_i) = (\Delta\vec{e}^{\,kl}(t_i))^T \hat{b}(t_i), \tag{24}$$

where $\Delta\vec{e}^{\,kl}(t_i)$ is obtained from the code solution with sufficient accuracy and $\hat{b}(t_i)$ is derived from the already calibrated phases.

MAXIMUM LIKELIHOOD (ML) AND MAXIMUM A POSTERIORI PROBABILITY (MAP) ESTIMATION OF AMBIGUITIES AND BASELINES

Measurement model

The double difference code and carrier phases $\Delta\rho^k_n$, $\Delta\varphi^k_n$ from K satellites $k \in \{1, \ldots, K\}$ at epoch $\{1, \ldots, s\}$ in block n and the a priori knowledge about the pitch angle $\overline{\nu}_1$, the rate of the pitch angle $\overline{\dot{\nu}}_1$, the heading $\overline{\nu}_2$, the rate of turn $\overline{\dot{\nu}}_2$, and the baseline length $\overline{l}$ shall be considered in a single measurement vector, which is modeled with equation (25), where $\Delta\boldsymbol{e}^k_n$ denotes the single difference of unit vectors pointing from satellite k and a reference satellite to the receiver, l_n is the true baseline length, $\nu_{1,n}$ and $\nu_{2,n}$ are the true pitch and heading angles, $\dot{\nu}_{1,n}$ and $\dot{\nu}_{2,n}$ are the respective rate of turns, $\boldsymbol{\xi}_n$ is the baseline in cartesian coordinates, $\boldsymbol{N}$ includes the integer ambiguities, λ is the wavelength of the carrier signal and $\boldsymbol{v}_n$ denotes the measurement noise. The vector of baselines $\boldsymbol{\xi}_n$ of s epochs is

$$\underbrace{\left[\begin{array}{c} \Delta\varphi_{n,1}^{1} \\ \vdots \\ \Delta\varphi_{n,1}^{K} \\ \hdashline \Delta\rho_{n,1}^{1} \\ \vdots \\ \Delta\rho_{n,1}^{K} \\ \hline \Delta\varphi_{n,2}^{1} \\ \vdots \\ \Delta\varphi_{n,2}^{K} \\ \hdashline \Delta\rho_{n,2}^{1} \\ \vdots \\ \Delta\rho_{n,2}^{K} \\ \hline \vdots \\ \hline \Delta\varphi_{n,s}^{1} \\ \vdots \\ \Delta\varphi_{n,s}^{K} \\ \hdashline \Delta\rho_{n,s}^{1} \\ \vdots \\ \Delta\rho_{n,s}^{K} \\ \hline \overline{\nu}_{1,n} \\ \dot{\overline{\nu}}_{1,n} \\ \overline{\nu}_{2,n} \\ \dot{\overline{\nu}}_{2,n} \\ \overline{l}_{n} \end{array}\right]}_{\boldsymbol{z}_n} = \underbrace{\left[\begin{array}{c|c|c|c|c|c} \Delta(\boldsymbol{e}_{n,1}^{1})^T & & & & \lambda & \\ \vdots & & & & \ddots & \\ \Delta(\boldsymbol{e}_{n,1}^{K})^T & & & & & \lambda \\ \hdashline \Delta(\boldsymbol{e}_{n,1}^{1})^T & & & & & \\ \vdots & & & & & \\ \Delta(\boldsymbol{e}_{n,1}^{K})^T & & & & & \\ \hline & \Delta(\boldsymbol{e}_{n,2}^{1})^T & & & \lambda & \\ & \vdots & & & \ddots & \\ & \Delta(\boldsymbol{e}_{n,2}^{K})^T & & & & \lambda \\ \hdashline & \Delta(\boldsymbol{e}_{n,2}^{1})^T & & & & \\ & \vdots & & & & \\ & \Delta(\boldsymbol{e}_{n,2}^{K})^T & & & & \\ \hline & & \ddots & & \vdots & \\ \hline & & & \Delta(\boldsymbol{e}_{n,s}^{1})^T & \lambda & \\ & & & \vdots & \ddots & \\ & & & \Delta(\boldsymbol{e}_{n,s}^{K})^T & & \lambda \\ \hdashline & & & \Delta(\boldsymbol{e}_{n,s}^{1})^T & & \\ & & & \vdots & & \\ & & & \Delta(\boldsymbol{e}_{n,s}^{K})^T & & \\ \hline & & & & & 1 \\ & & & & & \quad 1 \\ & & & & & \quad\quad 1 \\ & & & & & \quad\quad\quad 1 \\ & & & & & \quad\quad\quad\quad 1 \end{array}\right]}_{\boldsymbol{H}} \left[\begin{array}{c} \boldsymbol{\xi}_n \\ \hline \boldsymbol{N} \\ \hline \nu_{1,n} \\ \dot{\nu}_{1,n} \\ \nu_{2,n} \\ \dot{\nu}_{2,n} \\ l_n \end{array}\right] + \boldsymbol{v}_n, \tag{25}$$

modeled as

$$\boldsymbol{\xi}_n = \left[\begin{array}{c} l_n \cos(\nu_{1,n} + 1\delta t\dot{\nu}_{1,n}) \cos(\nu_{2,n} + 1\delta t\dot{\nu}_{2,n}) \\ l_n \cos(\nu_{1,n} + 1\delta t\dot{\nu}_{1,n}) \sin(\nu_{2,n} + 1\delta t\dot{\nu}_{2,n}) \\ l_n \sin(\nu_{1,n} + 1\delta t\dot{\nu}_{1,n}) \\ \hline l_n \cos(\nu_{1,n} + 2\delta t\dot{\nu}_{1,n}) \cos(\nu_{2,n} + 2\delta t\dot{\nu}_{2,n}) \\ l_n \cos(\nu_{1,n} + 2\delta t\dot{\nu}_{1,n}) \sin(\nu_{2,n} + 2\delta t\dot{\nu}_{2,n}) \\ l_n \sin(\nu_{1,n} + 2\delta t\dot{\nu}_{1,n}) \\ \hline \vdots \\ \hline l_n \cos(\nu_{1,n} + s\delta t\dot{\nu}_{1,n}) \cos(\nu_{2,n} + s\delta t\dot{\nu}_{2,n}) \\ l_n \cos(\nu_{1,n} + s\delta t\dot{\nu}_{1,n}) \sin(\nu_{2,n} + s\delta t\dot{\nu}_{2,n}) \\ l_n \sin(\nu_{1,n} + s\delta t\dot{\nu}_{1,n}) \end{array}\right], \tag{26}$$

with δt being the time interval between two measurements. The notation shall now be simplified by writing (25) as

$$\boldsymbol{z}_n = \boldsymbol{H} \cdot \left[\begin{array}{c} \boldsymbol{\xi}_n \\ \hline \boldsymbol{N} \\ \hline \nu_{1,n} \\ \dot{\nu}_{1,n} \\ \nu_{2,n} \\ \dot{\nu}_{2,n} \\ l_n \end{array}\right] + \boldsymbol{v}_n, \tag{27}$$

which includes two equivalent descriptions of the baseline vector, i.e. $\boldsymbol{\xi}_n$ in Cartesian coordinates and $\nu_{1,n}$, $\dot{\nu}_{1,n}$, $\nu_{2,n}$, $\dot{\nu}_{2,n}$ and l_n in spherical coordinates. To avoid linear dependencies, the measurements shall be expressed solely as a function of the spherical baseline parameters $\nu_{1,n}$, $\dot{\nu}_{1,n}$, $\nu_{2,n}$, $\dot{\nu}_{2,n}$, l_n and the ambiguities $\boldsymbol{N}$. Moreover, the measurement model shall be further strengthened by assuming a block-wise constant $\nu_{1,n}$, $\dot{\nu}_{1,n}$, $\nu_{2,n}$, $\dot{\nu}_{2,n}$ and l_n. These

extensions are reflected in the model

$$\boldsymbol{z}_n = \boldsymbol{h}_n(\boldsymbol{x}_n) + \boldsymbol{v}_n, \quad \text{with} \quad \boldsymbol{x}_n = \begin{bmatrix} \nu_{1,n} \\ \dot{\nu}_{1,n} \\ \nu_{2,n} \\ \dot{\nu}_{2,n} \\ l_n \\ \boldsymbol{N} \end{bmatrix}, \quad (28)$$

which includes 5 unknown real-valued parameters and K unknown integer ambiguities.

The non-linear function $\boldsymbol{h}_n(\boldsymbol{x}_n)$ is given by equation (29) and is obtained by replacing $\boldsymbol{\xi}_n$ in (25) by (26). Note that the a priori knowledge is modeled as a stochastic quantity in (25), i.e. a Gaussian distribution with mean values $\overline{\nu}_{1,n}$, $\overline{\dot{\nu}}_{1,n}$, $\overline{\nu}_{2,n}$, $\overline{\dot{\nu}}_{2,n}$, $\overline{l}_n$ and respective variances $\sigma^2_{\overline{\nu}_{1,n}}$, $\sigma^2_{\overline{\dot{\nu}}_{1,n}}$, $\sigma^2_{\overline{\nu}_{2,n}}$, $\sigma^2_{\overline{\dot{\nu}}_{2,n}}$ and $\sigma^2_{\overline{l}_n}$. The statistical modeling is advantageous as the true baseline parameters are not perfectly known in many applications. Consequently, a weighted least-squares baseline estimation based on the measurement model of (25) ensures a solution, which represents the optimum trade-off between low range residuals and a baseline close to the a priori knowledge.

MAP estimation of ambiguities and baselines

A Maximum Likelihood (ML) estimator tries to find the baseline parameters $\nu_{1,n}$, $\dot{\nu}_{1,n}$, $\nu_{2,n}$, $\dot{\nu}_{2,n}$, l_n and integer ambiguities $\boldsymbol{N}$, which have generated the measurements $\boldsymbol{z}_n$ with highest likelihood, i.e.

$$\max_{\nu_{1,n},\dot{\nu}_{1,n},\nu_{2,n},\dot{\nu}_{2,n},l_n} p(\boldsymbol{z}_n|\nu_{1,n},\dot{\nu}_{1,n},\nu_{2,n},\dot{\nu}_{2,n},l_n,\boldsymbol{N}) = \max_{\boldsymbol{x}_n} p(\boldsymbol{z}_n|\boldsymbol{x}_n). \quad (30)$$

An even more powerful estimator is the Maximum A Posteriori (MAP) probability estimator, which maximizes the probability of $\nu_{1,n}$, $\dot{\nu}_{1,n}$, $\nu_{2,n}$, $\dot{\nu}_{2,n}$ and l_n for a given $\boldsymbol{z}_n$. The MAP estimator is defined as

$$\max_{\boldsymbol{x}_n} p(\boldsymbol{x}_n|\boldsymbol{z}_n) = \max_{\boldsymbol{x}_n} p(\boldsymbol{z}_n|\boldsymbol{x}_n) \cdot \frac{p(\boldsymbol{x}_n)}{p(\boldsymbol{z}_n)}, \quad (31)$$

where the re-formulation is obtained with the rule of Bayes. The first (conditional) probability density describes the measurement noise, which is typically assumed to be Gaussian distributed, i.e.

$$p(\boldsymbol{z}_n|\boldsymbol{x}_n) = \frac{1}{\sqrt{(2\pi)^p|\boldsymbol{\Sigma}_n|}} e^{-\frac{1}{2}\|\boldsymbol{z}_n - \boldsymbol{h}_n(\boldsymbol{x}_n)\|^2_{\boldsymbol{\Sigma}_n^{-1}}}, \quad (32)$$

where $\boldsymbol{\Sigma}_n$ describes the covariance matrix of the measurement noise and $p = 2sK+5$. The second (joint) probability density of (31) describes the statistical a priori information about the baseline orientation/ length and integer ambiguities. This a priori information shall be assumed statistically independent, and Gaussian distributed with means according to the true baseline parameters, i.e.

$$\begin{aligned} p(\bar{\nu}_x) &= \frac{1}{\sqrt{2\pi\sigma^2_{\bar{\nu}_x}}} e^{-\frac{(\bar{\nu}_x - \nu_x)^2}{2\sigma^2_{\bar{\nu}_x}}}, \quad x \in \{1,2\} \\ p(\bar{\dot{\nu}}_x) &= \frac{1}{\sqrt{2\pi\sigma^2_{\bar{\dot{\nu}}_x}}} e^{-\frac{(\bar{\dot{\nu}}_x - \dot{\nu}_x)^2}{2\sigma^2_{\bar{\dot{\nu}}_x}}}, \quad x \in \{1,2\} \\ p(\bar{l}) &= \frac{1}{\sqrt{2\pi\sigma^2_{\bar{l}}}} e^{-\frac{(\bar{l}-l)^2}{2\sigma^2_{\bar{l}}}}, \\ p(\boldsymbol{N}) &= \frac{1}{\sqrt{2\pi|\boldsymbol{\Sigma}_{\bar{N}}|}} e^{-\frac{1}{2}\|\bar{\boldsymbol{N}} - \boldsymbol{N}\|^2_{\boldsymbol{\Sigma}_{\bar{N}}^{-1}}}. \end{aligned} \quad (33)$$

The third probability distribution (i.e. the one in the denominator) of (31) can be considered as a marginal distribution, i.e.

$$\begin{aligned} p(\boldsymbol{z}_n) = \iiiiiint & p(\boldsymbol{z}_n|\boldsymbol{x}_n) \\ & \cdot p(\nu_{1,n})p(\dot{\nu}_{1,n})p(\nu_{2,n})p(\dot{\nu}_{2,n})p(l_n) \\ & \cdot p(\boldsymbol{N}) d\nu_{1,n} d\dot{\nu}_{1,n} d\nu_{2,n} d\dot{\nu}_{2,n} dl_n d\boldsymbol{N}. \end{aligned} \quad (34)$$

The maximization of (31) can be simplified by taking the logarithm and omitting the pre-factor that does not depend on $\nu_{1,n}$, $\dot{\nu}_{1,n}$, $\nu_{2,n}$, $\dot{\nu}_{2,n}$ and l_n, i.e.

$$\begin{aligned} &\max_{\nu_{1,n},\dot{\nu}_{1,n},\nu_{2,n},\dot{\nu}_{2,n},l_n,\boldsymbol{N}} p(\nu_{1,n},\dot{\nu}_{1,n},\nu_{2,n},\dot{\nu}_{2,n},l_n,\boldsymbol{N}|\boldsymbol{z}_n) \\ &= \max_{\boldsymbol{x}_n} p(\boldsymbol{x}_n|\boldsymbol{z}_n) \\ &= \min_{\boldsymbol{x}_n} \Big(\|\boldsymbol{z}_n - \boldsymbol{h}_n(\boldsymbol{x}_n)\|^2_{\boldsymbol{\Sigma}_n^{-1}} \\ &\quad + \frac{(\nu_{1,n} - \bar{\nu}_{1,n})^2}{\sigma^2_{\bar{\nu}_{1,n}}} + \frac{(\dot{\nu}_{1,n} - \bar{\dot{\nu}}_{1,n})^2}{\sigma^2_{\bar{\dot{\nu}}_{1,n}}} \\ &\quad + \frac{(\nu_{2,n} - \bar{\nu}_{2,n})^2}{\sigma^2_{\bar{\nu}_{2,n}}} + \frac{(\dot{\nu}_{2,n} - \bar{\dot{\nu}}_{2,n})^2}{\sigma^2_{\bar{\dot{\nu}}_{2,n}}} \\ &\quad + \frac{(l_n - \bar{l}_n)^2}{\sigma^2_{\bar{l}}} + \|\boldsymbol{N} - \bar{\boldsymbol{N}}\|^2_{\boldsymbol{\Sigma}_N^{-1}} \Big), \end{aligned} \quad (35)$$

where the first term on the right side describes the squared range residuals and the remaining terms denote the squared deviation of the unknown baseline parameters from their a priori knowledge. In general, there is no a priori knowledge available for the ambiguities, such that the minimization simplifies to

$$\max_{\boldsymbol{x}_n} p(\boldsymbol{x}_n|\boldsymbol{z}_n) = \min_{\boldsymbol{x}_n} C(\boldsymbol{z}_n, \boldsymbol{x}_n) \quad (36)$$

$$\boldsymbol{h}_n(\boldsymbol{x}_n) = \boldsymbol{H} \cdot \begin{bmatrix} l_n \cos(\nu_{1,n} + 1 \cdot \delta t \cdot \dot{\nu}_{1,n}) \cos(\nu_{2,n} + 1 \cdot \delta t \cdot \dot{\nu}_{2,n}) \\ l_n \cos(\nu_{1,n} + 1 \cdot \delta t \cdot \dot{\nu}_{1,n}) \sin(\nu_{2,n} + 1 \cdot \delta t \cdot \dot{\nu}_{2,n}) \\ l_n \sin(\nu_{1,n} + 1 \cdot \delta t \cdot \dot{\nu}_{1,n}) \\ \hline l_n \cos(\nu_{1,n} + 2 \cdot \delta t \cdot \dot{\nu}_{1,n}) \cos(\nu_{2,n} + 2 \cdot \delta t \cdot \dot{\nu}_{2,n}) \\ l_n \cos(\nu_{1,n} + 2 \cdot \delta t \cdot \dot{\nu}_{1,n}) \sin(\nu_{2,n} + 2 \cdot \delta t \cdot \dot{\nu}_{2,n}) \\ l_n \sin(\nu_{1,n} + 2 \cdot \delta t \cdot \dot{\nu}_{1,n}) \\ \hline \vdots \\ \hline l_n \cos(\nu_{1,n} + s \cdot \delta t \cdot \dot{\nu}_{1,n}) \cos(\nu_{2,n} + s \cdot \delta t \cdot \dot{\nu}_{2,n}) \\ l_n \cos(\nu_{1,n} + s \cdot \delta t \cdot \dot{\nu}_{1,n}) \sin(\nu_{2,n} + s \cdot \delta t \cdot \dot{\nu}_{2,n}) \\ l_n \sin(\nu_{1,n} + s \cdot \delta t \cdot \dot{\nu}_{1,n}) \\ \hline N^1 \\ \vdots \\ N^K \\ \hline \nu_{1,n} \\ \dot{\nu}_{1,n} \\ \nu_{2,n} \\ \dot{\nu}_{2,n} \\ l_n \end{bmatrix} \tag{29}$$

with the cost function

$$\begin{aligned} C(\boldsymbol{z}_n, \boldsymbol{x}_n) &= \|\boldsymbol{z}_n - \boldsymbol{h}_n(\boldsymbol{x}_n)\|^2_{\boldsymbol{\Sigma}_n^{-1}} \\ &\quad + \frac{(\nu_{1,n} - \bar{\nu}_{1,n})^2}{\sigma^2_{\bar{\nu}_{1,n}}} + \frac{(\dot{\nu}_{1,n} - \bar{\dot{\nu}}_{1,n})^2}{\sigma^2_{\bar{\dot{\nu}}_{1,n}}} \\ &\quad + \frac{(\nu_{2,n} - \bar{\nu}_{2,n})^2}{\sigma^2_{\bar{\nu}_{2,n}}} + \frac{(\dot{\nu}_{2,n} - \bar{\dot{\nu}}_{2,n})^2}{\sigma^2_{\bar{\dot{\nu}}_{2,n}}} \\ &\quad + \frac{(l_n - \bar{l}_n)^2}{\sigma^2_{\bar{l}}}. \end{aligned} \tag{37}$$

Minimizing the cost function means that the derivatives have to be set to 0, i.e.

$$\begin{aligned} \frac{\partial C}{\partial \nu_{x,n}} &= 2 \cdot \|\boldsymbol{z}_n - \boldsymbol{h}_n(\boldsymbol{x}_n)\|_{\boldsymbol{\Sigma}_n^{-1}} \cdot \left(-\frac{\partial \boldsymbol{h}_n}{\partial \nu_{x,n}}\right) \\ &\quad - \frac{2(\nu_{x,n} - \bar{\nu}_{x,n})}{\sigma^2_{\bar{\nu}_{x,n}}} \stackrel{!}{=} 0, \quad x \in \{1,2\} \\ \frac{\partial C}{\partial \dot{\nu}_{x,n}} &= 2 \cdot \|\boldsymbol{z}_n - \boldsymbol{h}_n(\boldsymbol{x}_n)\|_{\boldsymbol{\Sigma}_n^{-1}} \cdot \left(-\frac{\partial \boldsymbol{h}_n}{\partial \dot{\nu}_{x,n}}\right) \\ &\quad - \frac{2(\dot{\nu}_{x,n} - \bar{\dot{\nu}}_{x,n})}{\sigma^2_{\bar{\dot{\nu}}_{x,n}}} \stackrel{!}{=} 0, \quad x \in \{1,2\} \\ \frac{\partial C}{\partial l_n} &= 2 \cdot \|\boldsymbol{z}_n - \boldsymbol{h}_n(\boldsymbol{x}_n)\|_{\boldsymbol{\Sigma}_n^{-1}} \cdot \left(-\frac{\partial \boldsymbol{h}_n}{\partial l_n}\right) \\ &\quad - \frac{2(l_n - \bar{l}_n)}{\sigma^2_{\bar{l}_n}} \stackrel{!}{=} 0 \\ \frac{\partial C}{\partial \boldsymbol{N}} &= 2 \cdot \|\boldsymbol{z}_n - \boldsymbol{h}_n(\boldsymbol{x}_n)\|_{\boldsymbol{\Sigma}_n^{-1}} \cdot \left(-\frac{\partial \boldsymbol{h}_n}{\partial \boldsymbol{N}}\right) \stackrel{!}{=} 0, \end{aligned} \tag{38}$$

which includes $K + 5$ partial derivatives.

The partial derivative w.r.t. the pitch angle $\nu_{1,n}$ is given by equation (39), the partial derivative w.r.t. the rate of turn $\dot{\nu}_{1,n}$ follows in equation (40), the partial derivative w.r.t. the heading $\nu_{2,n}$ is derived in equation (41) and the partial derivative w.r.t. the rate of turn $\dot{\nu}_{2,n}$ follows in equation (42). Finally, the partial derivatives w.r.t. the baseline length l_n and integer ambiguity N^k, $k \in \{1, \ldots, K\}$ are determined in equation (43). The system of equations of (38) can not be solved in closed form due to its non-linearity. Therefore, an iterative solution is computed with the Gauss-Newton method.

Iterative least-squares estimation with Gaussian a priori information about baseline length and attitude

The Gauss-Newton method is used to solve the system of equations (38) iteratively. In the $l \in \{1, \ldots, L\}$ th iteration, the baseline and float ambiguity estimates are obtained from

$$\begin{bmatrix} \hat{\nu}_{1,n}^{(l)} \\ \hat{\dot{\nu}}_{1,n}^{(l)} \\ \hat{\nu}_{2,n}^{(l)} \\ \hat{\dot{\nu}}_{2,n}^{(l)} \\ \hat{l}_n^{(l)} \\ \hat{\boldsymbol{N}}_n^{(l)} \end{bmatrix} = \begin{bmatrix} \hat{\nu}_{1,n}^{(l-1)} \\ \hat{\dot{\nu}}_{1,n}^{(l-1)} \\ \hat{\nu}_{2,n}^{(l-1)} \\ \hat{\dot{\nu}}_{2,n}^{(l-1)} \\ \hat{l}_n^{(l-1)} \\ \hat{\boldsymbol{N}}_n^{(l-1)} \end{bmatrix} - \boldsymbol{S}^{-1} \begin{bmatrix} \frac{\partial C}{\partial \nu_{1,n}} \\ \frac{\partial C}{\partial \dot{\nu}_{1,n}} \\ \frac{\partial C}{\partial \nu_{2,n}} \\ \frac{\partial C}{\partial \dot{\nu}_{2,n}} \\ \frac{\partial C}{\partial l_n} \\ \frac{\partial C}{\partial \boldsymbol{N}} \end{bmatrix}, \tag{44}$$

with the Hesse matrix defined in (45). The Gauss-Newton method is initialized by the converged state estimate of the

$$\frac{\partial \boldsymbol{h}_n}{\partial \nu_{1,n}} = \boldsymbol{H} \begin{bmatrix} -l_n \sin\left(\nu_{1,n} + 1 \cdot \delta t \cdot \dot{\nu}_{1,n}\right) \cos\left(\nu_{2,n} + 1 \cdot \delta t \cdot \dot{\nu}_{2,n}\right) \\ -l_n \sin\left(\nu_{1,n} + 1 \cdot \delta t \cdot \dot{\nu}_{1,n}\right) \sin\left(\nu_{2,n} + 1 \cdot \delta t \cdot \dot{\nu}_{2,n}\right) \\ l_n \cos\left(\nu_{1,n} + 1 \cdot \delta t \cdot \dot{\nu}_{1,n}\right) \\ \hline -l_n \sin\left(\nu_{1,n} + 2 \cdot \delta t \cdot \dot{\nu}_{1,n}\right) \cos\left(\nu_{2,n} + 2 \cdot \delta t \cdot \dot{\nu}_{2,n}\right) \\ -l_n \sin\left(\nu_{1,n} + 2 \cdot \delta t \cdot \dot{\nu}_{1,n}\right) \sin\left(\nu_{2,n} + 2 \cdot \delta t \cdot \dot{\nu}_{2,n}\right) \\ l_n \cos\left(\nu_{1,n} + 2 \cdot \delta t \cdot \dot{\nu}_{1,n}\right) \\ \hline \vdots \\ \hline -l_n \sin\left(\nu_{1,n} + s \cdot \delta t \cdot \dot{\nu}_{1,n}\right) \cos\left(\nu_{2,n} + s \cdot \delta t \cdot \dot{\nu}_{2,n}\right) \\ -l_n \sin\left(\nu_{1,n} + s \cdot \delta t \cdot \dot{\nu}_{1,n}\right) \sin\left(\nu_{2,n} + s \cdot \delta t \cdot \dot{\nu}_{2,n}\right) \\ l_n \cos\left(\nu_{1,n} + s \cdot \delta t \cdot \dot{\nu}_{1,n}\right) \\ \hline \mathbf{0} \\ \hline 1 \\ 0 \\ 0 \\ 0 \\ 0 \end{bmatrix}, \tag{39}$$

$$\frac{\partial \boldsymbol{h}_n}{\partial \dot{\nu}_{1,n}} = \boldsymbol{H} \begin{bmatrix} -l_n \sin\left(\nu_{1,n} + 1 \cdot \delta t \cdot \dot{\nu}_{1,n}\right) \cos\left(\nu_{2,n} + 1 \cdot \delta t \cdot \dot{\nu}_{2,n}\right) \cdot 1 \cdot \delta t \\ -l_n \sin\left(\nu_{1,n} + 1 \cdot \delta t \cdot \dot{\nu}_{1,n}\right) \sin\left(\nu_{2,n} + 1 \cdot \delta t \cdot \dot{\nu}_{2,n}\right) \cdot 1 \cdot \delta t \\ l_n \cos\left(\nu_{1,n} + 1 \cdot \delta t \cdot \dot{\nu}_{1,n}\right) \cdot 1 \cdot \delta t \\ \hline -l_n \sin\left(\nu_{1,n} + 2 \cdot \delta t \cdot \dot{\nu}_{1,n}\right) \cos\left(\nu_{2,n} + 2 \cdot \delta t \cdot \dot{\nu}_{2,n}\right) \cdot 2 \cdot \delta t \\ -l_n \sin\left(\nu_{1,n} + 2 \cdot \delta t \cdot \dot{\nu}_{1,n}\right) \sin\left(\nu_{2,n} + 2 \cdot \delta t \cdot \dot{\nu}_{2,n}\right) \cdot 2 \cdot \delta t \\ l_n \cos\left(\nu_{1,n} + 2 \cdot \delta t \cdot \dot{\nu}_{1,n}\right) \cdot 2 \cdot \delta t \\ \hline \vdots \\ \hline -l_n \sin\left(\nu_{1,n} + s \cdot \delta t \cdot \dot{\nu}_{1,n}\right) \cos\left(\nu_{2,n} + s \cdot \delta t \cdot \dot{\nu}_{2,n}\right) \cdot s \cdot \delta t \\ -l_n \sin\left(\nu_{1,n} + s \cdot \delta t \cdot \dot{\nu}_{1,n}\right) \sin\left(\nu_{2,n} + s \cdot \delta t \cdot \dot{\nu}_{2,n}\right) \cdot s \cdot \delta t \\ l_n \cos\left(\nu_{1,n} + s \cdot \delta t \cdot \dot{\nu}_{1,n}\right) \cdot s \cdot \delta t \\ \hline \mathbf{0} \\ \hline 0 \\ 1 \\ 0 \\ 0 \\ 0 \end{bmatrix} \tag{40}$$

previous block, i.e.

$$\begin{bmatrix} \hat{\nu}_{1,n}^{(1)} \\ \hat{\nu}_{2,n}^{(1)} \\ \hat{\dot{\nu}}_{2,n}^{(1)} \\ \hat{l}_n^{(1)} \\ \hat{\boldsymbol{N}}_n^{(1)} \end{bmatrix} = \begin{bmatrix} \hat{\nu}_{1,n-1}^{(L)} \\ \hat{\nu}_{2,n-1}^{(L)} \\ \hat{\dot{\nu}}_{2,n-1}^{(L)} \\ \hat{l}_{n-1}^{(L)} \\ \hat{\boldsymbol{N}}_{n-1}^{(L)} \end{bmatrix}. \tag{46}$$

The iterative Newton method does not necessarily converge to the global optimum due to the nonlinearity of the cost function C. However, one can repeat the computation for a few random initializations around the a priori information, and select the one with minimum C to increase the probability of finding the global minimum.

Fig. 11 shows the benefit of tight and soft baseline length constraints for integer least-squares estimation (ILS): The tight constraint (TC) reduces the probability of wrong unconstrained fixing by more than four orders of magnitude if the a priori length information is correct. The error rates are based on a simulation of Galileo double difference phase measurements on E1 and E5 of 4 epochs for a short baseline of 30 m. Phase-only measurements were considered to avoid code multipath, and a widelane combination with a wavelength of 78.1 cm was used to increase the success rate. A satellite geometry with 8 visible satellites was selected to obtain a typical performance. Obviously, the tight constraint makes the fixing also sensitive w.r.t. erroneous a priori information, i.e. it degrades the unconstrained performance if the error in the a priori information exceeds 50 cm. The soft constrained (SC) fixing takes the uncertainty

$$\frac{\partial \boldsymbol{h}}{\partial \nu_{2,n}} = \boldsymbol{H} \begin{bmatrix} -l_n \cos\left(\nu_{1,n} + 1 \cdot \delta t \cdot \dot{\nu}_{1,n}\right) \sin\left(\nu_{2,n} + 1 \cdot \delta t \cdot \dot{\nu}_{2,n}\right) \\ l_n \cos\left(\nu_{1,n} + 1 \cdot \delta t \cdot \dot{\nu}_{1,n}\right) \cos\left(\nu_{2,n} + 1 \cdot \delta t \cdot \dot{\nu}_{2,n}\right) \\ 0 \\ \hline -l_n \cos\left(\nu_{1,n} + 2 \cdot \delta t \cdot \dot{\nu}_{1,n}\right) \sin\left(\nu_{2,n} + 2 \cdot \delta t \cdot \dot{\nu}_{2,n}\right) \\ l_n \cos\left(\nu_{1,n} + 2 \cdot \delta t \cdot \dot{\nu}_{1,n}\right) \cos\left(\nu_{2,n} + 2 \cdot \delta t \cdot \dot{\nu}_{2,n}\right) \\ 0 \\ \hline \vdots \\ \hline -l_n \cos\left(\nu_{1,n} + s \cdot \delta t \cdot \dot{\nu}_{1,n}\right) \sin\left(\nu_{2,n} + s \cdot \delta t \cdot \dot{\nu}_{2,n}\right) \\ l_n \cos\left(\nu_{1,n} + s \cdot \delta t \cdot \dot{\nu}_{1,n}\right) \cos\left(\nu_{2,n} + s \cdot \delta t \cdot \dot{\nu}_{2,n}\right) \\ 0 \\ \hline \mathbf{0} \\ \hline 0 \\ 0 \\ 1 \\ 0 \\ 0 \end{bmatrix} \tag{41}$$

$$\frac{\partial \boldsymbol{h}}{\partial \dot{\nu}_{2,n}} = \boldsymbol{H} \begin{bmatrix} -l_n \cos\left(\nu_{1,n} + 1 \cdot \delta t \cdot \dot{\nu}_{1,n}\right) \sin\left(\nu_{2,n} + 1 \cdot \delta t \cdot \dot{\nu}_{2,n}\right) \cdot 1 \cdot \delta t \\ l_n \cos\left(\nu_{1,n} + 1 \cdot \delta t \cdot \dot{\nu}_{1,n}\right) \cos\left(\nu_{2,n} + 1 \cdot \delta t \cdot \dot{\nu}_{2,n}\right) \cdot 1 \cdot \delta t \\ 0 \\ \hline -l_n \cos\left(\nu_{1,n} + 2 \cdot \delta t \cdot \dot{\nu}_{1,n}\right) \sin\left(\nu_{2,n} + 2 \cdot \delta t \cdot \dot{\nu}_{2,n}\right) \cdot 2 \cdot \delta t \\ l_n \cos\left(\nu_{1,n} + 2 \cdot \delta t \cdot \dot{\nu}_{1,n}\right) \cos\left(\nu_{2,n} + 2 \cdot \delta t \cdot \dot{\nu}_{2,n}\right) \cdot 2 \cdot \delta t \\ 0 \\ \hline \vdots \\ \hline -l_n \cos\left(\nu_{1,n} + s \cdot \delta t \cdot \dot{\nu}_{1,n}\right) \sin\left(\nu_{2,n} + s \cdot \delta t \cdot \dot{\nu}_{2,n}\right) \cdot s \cdot \delta t \\ l_n \cos\left(\nu_{1,n} + s \cdot \delta t \cdot \dot{\nu}_{1,n}\right) \cos\left(\nu_{2,n} + s \cdot \delta t \cdot \dot{\nu}_{2,n}\right) \cdot s \cdot \delta t \\ 0 \\ \hline \mathbf{0} \\ \hline 0 \\ 0 \\ 0 \\ 1 \\ 0 \end{bmatrix} \tag{42}$$

in the length information into account and, thereby, improves the unconstrained fixing for any quality of the a priori information.

Fig. 12 and 13 show the achievable accuracies for soft constrained estimation of a vertical baseline with $l = 10$ m.

The minimization of the cost function of (37) ensures an optimal trade-off between the minimization of the weighted range residuals and the minimization of the weighted difference between the estimated baseline parameters and their a priori knowledge. Consequently, the achievable accuracies depend on the accuracy of the double difference measurements (or, more specifically, on the accuracy of the widelane phase-only combination with $\lambda = 78.1$ cm) and the accuracy of the a priori information ($\sigma_{\nu_1} = 30°$, $\sigma_{\nu_2} = \infty$, $\sigma_l = 10\mathrm{cm}$). Obviously, the elevation of the baseline can be determined with a higher accuracy than the length due to the relatively long baseline.

Improving accuracy and reliability of attitude determination with state space model and Kalman filtering

The accuracy of joint baseline and ambiguity estimation can be improved by a state space model, which describes the movement of receivers. Such a state space model can be especially tight for maritime navigation due the large inertia of ships. Assuming Gauss-Markov processes for the rates $\{\dot{\nu}_{1,n}, \dot{\nu}_{2,n}\}$ and the baseline length l_n, the state space

$$\frac{\partial \boldsymbol{h}}{\partial l_n} = \boldsymbol{H} \begin{bmatrix} \cos\left(\nu_{1,n} + 1 \cdot \delta t \cdot \dot{\nu}_{1,n}\right) \cos\left(\nu_{2,n} + 1 \cdot \delta t \cdot \dot{\nu}_{2,n}\right) \\ \cos\left(\nu_{1,n} + 1 \cdot \delta t \cdot \dot{\nu}_{1,n}\right) \sin\left(\nu_{2,n} + 1 \cdot \delta t \cdot \dot{\nu}_{2,n}\right) \\ \sin\left(\nu_{1,n} + 1 \cdot \delta t \cdot \dot{\nu}_{1,n}\right) \\ \hline \cos\left(\nu_{1,n} + 2 \cdot \delta t \cdot \dot{\nu}_{1,n}\right) \cos\left(\nu_{2,n} + 2 \cdot \delta t \cdot \dot{\nu}_{2,n}\right) \\ \cos\left(\nu_{1,n} + 2 \cdot \delta t \cdot \dot{\nu}_{1,n}\right) \sin\left(\nu_{2,n} + 2 \cdot \delta t \cdot \dot{\nu}_{2,n}\right) \\ \sin\left(\nu_{1,n} + 2 \cdot \delta t \cdot \dot{\nu}_{1,n}\right) \\ \hline \vdots \\ \hline \cos\left(\nu_{1,n} + s \cdot \delta t \cdot \dot{\nu}_{1,n}\right) \cos\left(\nu_{2,n} + s \cdot \delta t \cdot \dot{\nu}_{2,n}\right) \\ \cos\left(\nu_{1,n} + s \cdot \delta t \cdot \dot{\nu}_{1,n}\right) \sin\left(\nu_{2,n} + s \cdot \delta t \cdot \dot{\nu}_{2,n}\right) \\ \sin\left(\nu_{1,n} + s \cdot \delta t \cdot \dot{\nu}_{1,n}\right) \\ \hline \mathbf{0} \\ \hline 0 \\ 0 \\ 0 \\ 0 \\ 1 \end{bmatrix}, \qquad \frac{\partial \boldsymbol{h}}{\partial N^k} = \boldsymbol{H} \begin{bmatrix} 0 \\ 0 \\ 0 \\ \hline 0 \\ 0 \\ 0 \\ \hline \vdots \\ \hline 0 \\ 0 \\ 0 \\ \hline \mathbf{0}^{k-1\times 1} \\ 1 \\ \mathbf{0}^{K-k\times 1} \\ \hline 0 \\ \vdots \\ 0 \end{bmatrix} \tag{43}$$

$$\boldsymbol{S} = \begin{bmatrix} \frac{\partial^2 C}{\partial^2 \nu_{1,n}} & \frac{\partial^2 C}{\partial \nu_{1,n} \partial \dot{\nu}_{1,n}} & \frac{\partial^2 C}{\partial \nu_{1,n} \partial \nu_{2,n}} & \frac{\partial^2 C}{\partial \nu_{1,n} \partial \dot{\nu}_{2,n}} & \frac{\partial^2 C}{\partial \nu_{1,n} \partial l_n} & \frac{\partial^2 C}{\partial \nu_{1,n} \partial \boldsymbol{N}} \\ \frac{\partial^2 C}{\partial \dot{\nu}_{1,n} \partial \nu_{1,n}} & \frac{\partial^2 C}{\partial^2 \dot{\nu}_{1,n}} & \frac{\partial^2 C}{\partial \dot{\nu}_{1,n} \partial \nu_{2,n}} & \frac{\partial^2 C}{\partial \dot{\nu}_{1,n} \partial \dot{\nu}_{2,n}} & \frac{\partial^2 C}{\partial \dot{\nu}_{1,n} \partial l_n} & \frac{\partial^2 C}{\partial \dot{\nu}_{1,n} \partial \boldsymbol{N}} \\ \frac{\partial^2 C}{\partial \nu_{2,n} \partial \nu_{1,n}} & \frac{\partial^2 C}{\partial \nu_{2,n} \partial \dot{\nu}_{1,n}} & \frac{\partial^2 C}{\partial^2 \nu_{2,n}} & \frac{\partial^2 C}{\partial \nu_{2,n} \partial \dot{\nu}_{2,n}} & \frac{\partial^2 C}{\partial \nu_{2,n} l_n} & \frac{\partial^2 C}{\partial \nu_{2,n} \partial \boldsymbol{N}} \\ \frac{\partial^2 C}{\partial \dot{\nu}_{2,n} \partial \nu_{1,n}} & \frac{\partial^2 C}{\partial \dot{\nu}_{2,n} \partial \dot{\nu}_{1,n}} & \frac{\partial^2 C}{\partial \dot{\nu}_{2,n} \partial \nu_{2,n}} & \frac{\partial^2 C}{\partial^2 \dot{\nu}_{2,n}} & \frac{\partial^2 C}{\partial \dot{\nu}_{2,n} \partial l_n} & \frac{\partial^2 C}{\partial \dot{\nu}_{2,n} \partial \boldsymbol{N}} \\ \frac{\partial^2 C}{\partial l_n \partial \nu_{1,n}} & \frac{\partial^2 C}{\partial l_n \partial \dot{\nu}_{1,n}} & \frac{\partial^2 C}{\partial l_n \partial \nu_{2,n}} & \frac{\partial^2 C}{\partial l_n \partial \dot{\nu}_{2,n}} & \frac{\partial^2 C}{\partial^2 l_n} & \frac{\partial^2 C}{\partial l_n \partial \boldsymbol{N}} \\ \frac{\partial^2 C}{\partial \boldsymbol{N} \partial \nu_{1,n}} & \frac{\partial^2 C}{\partial \boldsymbol{N} \partial \dot{\nu}_{1,n}} & \frac{\partial^2 C}{\partial \boldsymbol{N} \partial \nu_{2,n}} & \frac{\partial^2 C}{\partial \boldsymbol{N} \partial \dot{\nu}_{2,n}} & \frac{\partial^2 C}{\partial \boldsymbol{N} \partial l_n} & \frac{\partial^2 C}{\partial^2 \boldsymbol{N}} \end{bmatrix} \tag{45}$$

model is obtained as

$$\underbrace{\begin{bmatrix} \nu_{1,n} \\ \dot{\nu}_{1,n} \\ \nu_{2,n} \\ \dot{\nu}_{2,n} \\ l_n \\ \boldsymbol{N} \end{bmatrix}}_{\boldsymbol{x}_n} = \underbrace{\left[\begin{array}{cc|cc|c} 1 & s \cdot \delta t & & & \\ & 1 & & & \\ \hline & & 1 & s \cdot \delta t & \\ & & & 1 & \\ \hline & & & & \begin{array}{cc} 1 & \\ & \mathbf{1} \end{array} \end{array}\right]}_{\boldsymbol{\Phi}} \underbrace{\begin{bmatrix} \nu_{1,n-1} \\ \dot{\nu}_{1,n-1} \\ \nu_{2,n-1} \\ \dot{\nu}_{2,n-1} \\ l_{n-1} \\ \boldsymbol{N} \end{bmatrix}}_{\boldsymbol{x}_{n-1}} + \underbrace{\begin{bmatrix} w_{\nu_{1,n}} \\ w_{\dot{\nu}_{1,n}} \\ w_{\nu_{2,n}} \\ w_{\dot{\nu}_{2,n}} \\ w_{l_n} \\ w_{\boldsymbol{N}} \end{bmatrix}}_{\boldsymbol{w}_n}. \tag{47}$$

This state space model is included into the MAP estimation by a Kalman filter, which combines the GNSS measurements, the a priori information and the state space model. The Kalman filter includes a linear prediction of the state estimate from one block to the next one, i.e.

$$\begin{aligned} \hat{\boldsymbol{x}}_{n+1}^{-} &= \boldsymbol{\Phi}_n \hat{\boldsymbol{x}}_n^{+} \\ \boldsymbol{P}_{\hat{\boldsymbol{x}}_{n+1}^{-}} &= \boldsymbol{\Phi}_n \boldsymbol{P}_{\hat{\boldsymbol{x}}_n^{+}} \boldsymbol{\Phi}_n^T + \boldsymbol{Q}_{n+1}, \end{aligned} \tag{48}$$

where the second row describes the process noise covariance matrix obtained by error propagation. Once the new measurement is available, the state estimate is updated, i.e.

$$\hat{\boldsymbol{x}}_n^{+} = \hat{\boldsymbol{x}}_n^{-} + \boldsymbol{K}_n \left(\boldsymbol{z}_n - \boldsymbol{h}_n(\hat{\boldsymbol{x}}_n^{-}) \right), \tag{49}$$

where $\boldsymbol{K}_n$ is the Kalman gain, which is computed such that the variance of the norm of the a posteriori state estimate is minimized, i.e.

$$\boldsymbol{K}_n = \arg\min_{K_n} \mathrm{E}\{\|\hat{\boldsymbol{x}}_n^{+} - \mathrm{E}\{\hat{\boldsymbol{x}}_n^{+}\}\|^2\}. \tag{50}$$

This minimization of a variance of a highly non-linear function of Gaussian random variables can not be performed in closed form. Therefore, the function $\boldsymbol{h}_n(\boldsymbol{x}_n)$ is linearized around an initial state $\boldsymbol{x}_0$, as written in equation (51), where the partial derivatives are given in (39)-(43) in closed form, and can be stacked into a single matrix:

$$\boldsymbol{H}_n = \left[\frac{\partial \boldsymbol{h}}{\partial \nu_{1,n}} \quad \frac{\partial \boldsymbol{h}}{\partial \dot{\nu}_{1,n}} \quad \frac{\partial \boldsymbol{h}}{\partial \nu_{2,n}} \quad \frac{\partial \boldsymbol{h}}{\partial \dot{\nu}_{2,n}} \quad \frac{\partial \boldsymbol{h}}{\partial l} \quad \frac{\partial \boldsymbol{h}}{\partial \boldsymbol{N}^1} \cdots \frac{\partial \boldsymbol{h}}{\partial \boldsymbol{N}^K} \right]. \tag{52}$$

This linearization of $\boldsymbol{h}_n(\boldsymbol{x}_n)$ enables the solution of (50) in closed form:

$$\boldsymbol{K}_n = \boldsymbol{P}_{\hat{\boldsymbol{x}}_n^{-}} \boldsymbol{H}_n^T \left(\boldsymbol{H}_n \boldsymbol{P}_{\hat{\boldsymbol{x}}_n^{-}} \boldsymbol{H}_n^T + \boldsymbol{\Sigma}_n \right)^{-1}, \tag{53}$$

$$\boldsymbol{h}_n(\boldsymbol{x}_n) = \boldsymbol{h}_n(\boldsymbol{x}_0) + \left.\frac{\partial \boldsymbol{h}(\boldsymbol{x})}{\partial \nu_1}\right|_{\boldsymbol{x}=\boldsymbol{x}_0} \cdot (\nu_{1,n} - \nu_{1,0}) + \left.\frac{\partial \boldsymbol{h}(\boldsymbol{x})}{\partial \dot{\nu}_1}\right|_{\boldsymbol{x}=\boldsymbol{x}_0} \cdot (\dot{\nu}_{1,n} - \dot{\nu}_{1,0}) + \left.\frac{\partial \boldsymbol{h}(\boldsymbol{x})}{\partial \nu_2}\right|_{\boldsymbol{x}=\boldsymbol{x}_0} \cdot (\nu_{2,n} - \nu_{2,0}) + \left.\frac{\partial \boldsymbol{h}(\boldsymbol{x})}{\partial \dot{\nu}_2}\right|_{\boldsymbol{x}=\boldsymbol{x}_0} \cdot (\dot{\nu}_{2,n} - \dot{\nu}_{2,0}) + \left.\frac{\partial \boldsymbol{h}(\boldsymbol{x})}{\partial l}\right|_{\boldsymbol{x}=\boldsymbol{x}_0} \cdot (l_n - l_0) + \sum_{k=1}^{K} \left(\left.\frac{\partial \boldsymbol{h}(\boldsymbol{x})}{\partial N^k}\right|_{\boldsymbol{x}=\boldsymbol{x}_0} \cdot (N_n^k - N_0^k) \right) \quad (51)$$

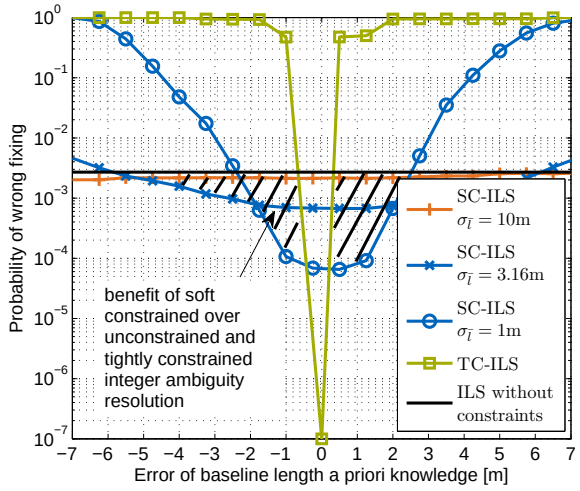

Fig. 11 Comparison of unconstrained, soft constrained and tightly constrained ambiguity resolution for erroneous baseline length a priori information: The tightly constrained ambiguity resolution outperforms the unconstrained and soft constrained fixing for perfect a priori knowledge but is extremely sensitive w.r.t. erroneous a priori information. The soft constrained ambiguity fixing benefits from the a priori information even if it is biased.

where $\boldsymbol{\Sigma}_n$ denotes the covariance matrix of the measurement noise $\boldsymbol{v}_n$.

The benefit of Gaussian a priori knowledge for the Kalman filter based estimation of ambiguities and baseline shall now be analyzed for inland water navigation. In this case, the rate of pitch $\dot{\nu}_{1,n}$ becomes negligible and, thus, is set to 0 and excluded from the state space vector. We process 5 Hz single frequency code and carrier phase measurements, which are grouped in blocks of $s = 5$ epochs to make the rate of the heading observable. The single difference unit vectors $\Delta \boldsymbol{e}_n^k$ are computed from a snapshot of 8 visible satellites as observable at Advanced Navigation Solutions - ANAVS once the full Galileo 27/3/1 Walker constellation becomes operational. The assumptions of the baseline, measurement and process noises, and of the a priori knowledge are summarized in Tab. 1, and are considered typical for inland water navigation with low cost receivers. The uncertainty in the baseline length arises from a non perfect coupling of cargo ships and/ or antenna phase center variations.

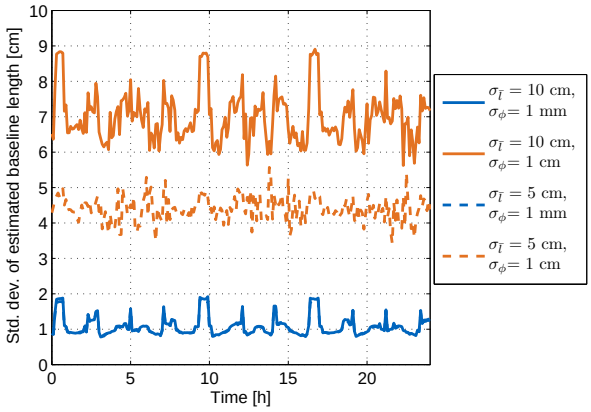

Fig. 12 Soft constrained estimation of baseline length for $l = 10$ m and $\nu_1 = 90°$: The achievable accuracy depends on the noise level of the measurements, the noise amplifications due to double differencing, widelane combinations and the geometry, and the quality of the a priori information. The latter one becomes especially beneficial for an increased phase noise level.

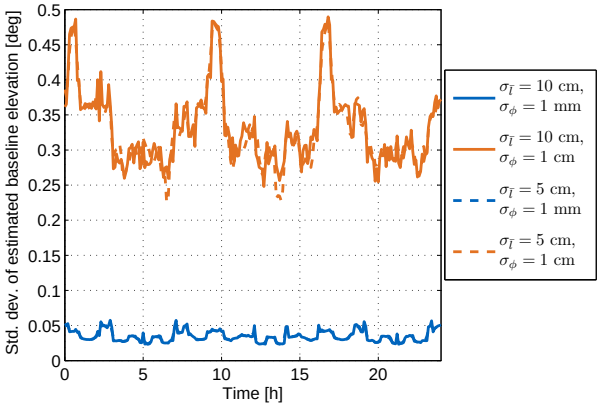

Fig. 13 Soft constrained estimation of baseline elevation for $l = 10$ m and $\nu_1 = 90°$: The a priori knowledge has only a minor impact on the estimation of the elevation due to the large baseline length, which enables a precise computation of its elevation.

Fig. 14a shows the convergence of the constrained a posteriori float ambiguity estimates for $\sigma_{\bar{l}} = 5$ cm but no a priori knowledge about the pitch angle. In this case, it ta-

Tab. 1 Simulation scenario for inland water navigation

Initial baseline	$l_0 = 100\,\mathrm{m}$, $\nu_{1,0} = 2°$, $\nu_{2,0} = 45°$, $\dot{\nu_{2,0}} = 1°/\mathrm{s}$
Measurement noise	$\sigma_\varphi = 1\mathrm{cm}$, $\sigma_\rho = 1\mathrm{m}$
Process noise	$\sigma_{\nu_1} = 0.001°$, $\sigma_{\dot{\nu}_2} = 0.03°/\delta t$, $\sigma_l = 0$, $\delta t = 0.2\mathrm{s}$
Baseline a priori knowledge	
Length	$\sigma_{\bar{l}} = 5\mathrm{cm}$
Pitch angle, Fig. 14	$\sigma_{\bar{\nu}_1} = \infty$
Pitch angle, Fig. 15	$\sigma_{\bar{\nu}_1} = 0.1°$

kes 140 s until all float ambiguity estimates are at most 0.1 cycles apart from an integer number. The reduction of the float ambiguity errors within this time span clearly indicates the benefit of the state space model and a Kalman filter. Fig. 14b shows the convergence process of the constrained a posteriori baseline parameters for the same simulation scenario. The estimate of ν_1 is much more noisy than the one of ν_2, which is a consequence of the geometry: The sensitivity of the cost function C w.r.t. $\nu_{1,n}$ at $\nu_{1_0} = 2°$ is much smaller than the sensitivity w.r.t. $\nu_{2,n}$ at $\nu_{2_0} = 45°$, which results in a noisier estimate. One can also observe the process noise after the convergence is reached.

Fig. 15 show the benefit of an improved a priori knowledge of the pitch angle: The reduction of the uncertainty to $\sigma_{\bar{\nu}_1} = 0.1°$ (which corresponds to a length uncertainty of 17.4 cm for $l = 100\,\mathrm{m}$) substantially shortens the convergence process, and enables reliable float ambiguities and baseline estimates within less than 10 epochs (i.e. 2s).

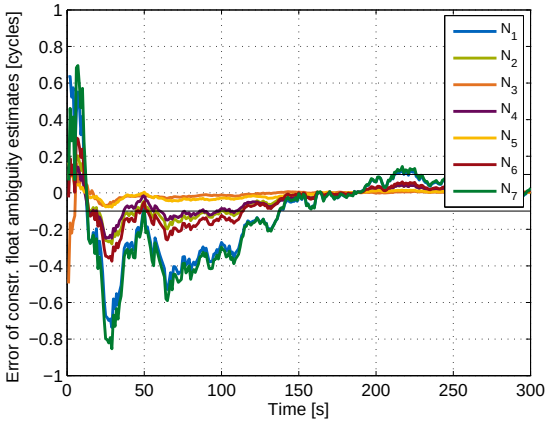

(a) Float ambiguity estimates

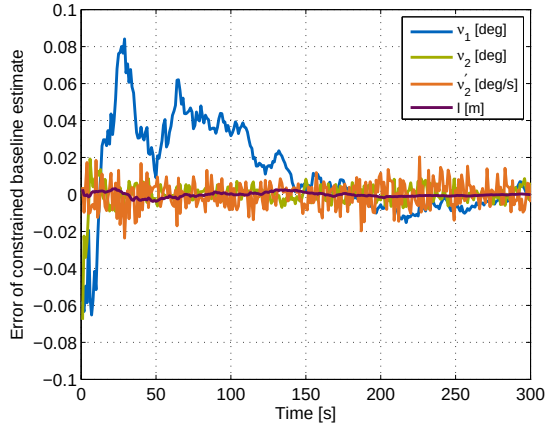

(b) Spherical baseline estimates

Fig. 14 Convergence of constrained ambiguity and baseline estimates for Gaussian a priori knowledge with $\sigma_{\bar{l}} = 5\mathrm{cm}$, $\sigma_{\bar{\nu}_1} = \infty$.

CONCLUSION

First, a new method for heading estimation with kinematic phase calibration was proposed and tested with two low cost navigation chips/ antennas, that typically suffer from an unreliable phase tracking. The proposed method lumps the double difference integer ambiguities, the double difference atmospheric delays, and the double difference clock offsets to a single bias, which is determined (and updated) during kinematic phase calibrations. The achievable accuracy is $0.5°/$ baseline length, i.e. $0.5°$ for a baseline length of 1 m and $0.005°$ for a baseline length of 100 m, and only limited by the phase noise.

These kinematic calibrations start with a conventional absolute position estimation based on the iterative least-squares method and pseudorange measurements. The actual phase calibration is then performed in three steps: First, a smoothed receiver trajectory is calculated either by a polynomial fitting or by a map matching of the absolute position estimates. In a second step, the baseline vector between both receivers is calibrated based on the smoothed receiver trajectory and the a priori known baseline length and elevation. In the third step, the double difference carrier phases are calibrated based on the smoothed receiver trajectory and the direction vectors pointing from the satellites to the receivers. Once a sufficiently large number of carrier phase is calibrated, cycle slips and other phase jumps are detected and corrected for the remaining satellites based on the history of the calibrated phases and their extrapolation.

Second, a maximum likelihood estimation of ambiguities and baselines was proposed for reliable differential carrier phase positioning. It uses Gaussian a priori knowledge of the baseline length and pitch angle, and performs a recursive least-squares estimation with a Kalman filter to obtain the float solution. It is shown that the maximum a posteriori probability estimator finds the optimum trade-off between a solution, which only minimizes the range residuals and one, which only minimizes the distance to the a priori information. The obtained simulation results show that the Gaussian a priori knowledge enables a ten times faster convergence of the float solution compared to the one without a priori information and that it allows some errors in

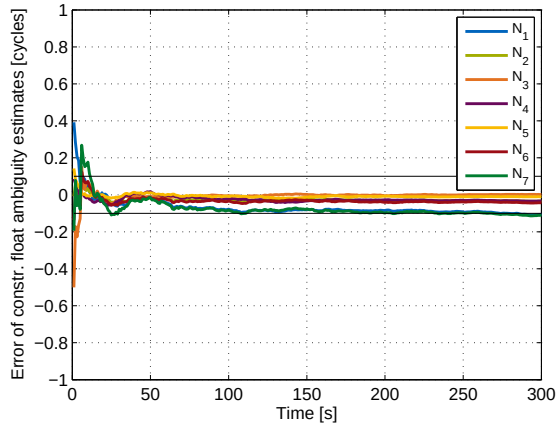

(a) Float ambiguity estimates

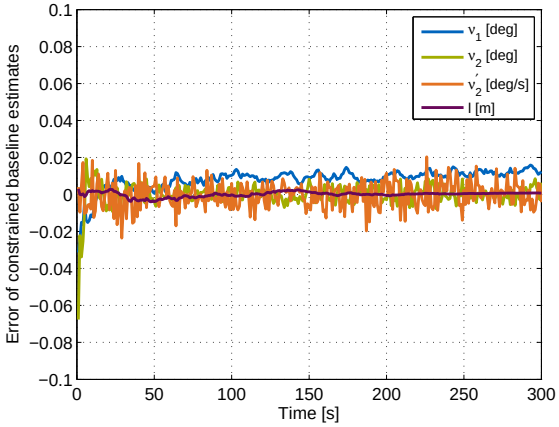

(b) Spherical baseline estimates

Fig. 15 Convergence of constrained ambiguity and baseline estimates for Gaussian a priori knowledge with $\sigma_{\bar{l}} = 5\text{cm}$, $\sigma_{\bar{\nu}_1} = 0.1°$.

the a priori information, i.e. it is much more robust than deterministic a priori knowledge.

ACKNOWLEDGEMENTS

The first author would like to thank the Projektträger Jülich (PTJ) for an EXIST scholarship and the financial support of this trip. The second author would like to thank the German Federal Ministry of Economic Affairs and Technology (BMWi) and the German Aerospace Center (DLR) for a financial grant (FKZ: 50NA1104) to the project LINGAT which supported this work.

Furthermore, the authors would like to thank Dr. v. Hinüber, Mr. Scheyer and Dr. Stefan Knedlik from iMAR for a joint measurement campaign and many fruitful discussions.

REFERENCES

[1] P. Jurkowski, Reliable attitude determination with GNSS: Gaussian a priori knowledge and Kalman filtering, *Diplomarbeit*, Technische Universität München, 53 pp., **2011**.

[2] P. Jurkowski, P. Henkel, G. Gao, and C. Günther, Integer Ambiguity Resolution with Tight and Soft Baseline Constraints for Freight Stabilization at Helicopters and Cranes, *Proc. of ION ITM*, San Diego, USA, pp. 336-346, **Jan. 2011**.

[3] P. Henkel, P. Jurkowski and C. Günther, Differential integer ambiguity resolution with Gaussian a priori knowledge and Kalman filtering, *Proc. of ION GNSS*, **Sep. 2011**

[4] P. Henkel and C. Günther, Reliable Integer Ambiguity Resolution with Multi-frequency Mixed Code Carrier Combinations, *Journal of Global Positioning Systems*, Vol.9, No.2: 90-103, **2010**.

[5] P. Henkel, Reliable Carrier Phase Positioning, *PhD thesis*, Verlag Dr. Hut, München, 177 pp., **2010**.

[6] P. Henkel and C. Günther, Reliable Carrier Phase Positioning with Multi-Frequency Code Carrier Linear Combinations, *Proc. of 23rd ION Intern. Techn. Meet.* (ION-GNSS), Portland, USA, **2010**.

[7] P. Jurkowski, Baseline constrained ambiguity resolution with multiple frequencies, *Bachelor thesis*, Technische Universität München, 49 pp., **2010**.

[8] P. Teunissen, The least-squares ambiguity decorrelation adjustment: a method for fast GPS ambiguity estimation, *J. of Geodesy*, vol. 70, pp. 65-82, **1995**.

[9] P. Teunissen, The LAMBDA method for the GNSS compass, *Art. Satellites*, vol. 41, nr. 3, pp. 89-103, **2006**.

[10] P. Teunissen, Integer least-squares theory for the GNSS compass, *J. of Geodesy*, vol. 84, pp. 433-447, **2010**.

[11] P. Misra and P. Enge, Global Positioning System, *Ganga-Jamuna Press*, **2006**

[12] G. Strang and K. Borre, Linear algebra, geodesy, and GPS, *Wellesley-Cambridge Press*, **1997**